Passage from Spin-Polarized Surface States to Unpolarized Quantum Well States in Topologically Nontrivial Sb Films

G. Bian, T. Miller, and T.-C. Chiang

Passage from Spin-Polarized Surface States to Unpolarized Quantum Well States in Topologically Nontrivial Sb Films

G. Bian, T. Miller, and T.-C. Chiang

Department of Physics, University of Illinois at Urbana-Champaign, 1110 West Green Street,

Urbana, Illinois 61801-3080, USA,

and Frederick Seitz Materials Research Laboratory, University of Illinois at Urbana-Champaign,

104 South Goodwin Avenue, Urbana, Illinois 61801-2902, USA

Topological materials have unusual surface spin properties including a net surface spin current protected by the bulk symmetry properties. When such materials are reduced to thin films, their gapless spin-polarized surface states must connect, by analytic continuation, to bulk-derived quantum well states, which are spin-unpolarized in centrosymmetric systems. The nature of this passage in a model system, Sb films, is investigated. Angle-resolved photoemission shows a smooth transition, while calculations elucidate the correlated evolution of the spin and charge distributions in real space.

Topological insulators are characterized by a strong spin-orbit coupling that leads to a set of spin-split surface states with special connections to bulk states [1,2,3,4,5,6,7,8]. In the simplest case where just one pair of spin-split surface states exist in the gap, one of them must disperse into the bulk conduction band, and the other must disperse into the bulk valence band. The bulk gap is thus completely spanned by metallic surface states that carry a net spin current. Whereas the surfaces of bulk topological insulators provide a promising basis for spintronics applications for this reason, thin films are more relevant to actual device architecture. This paper considers the mesoscopic regime where the film thickness is sufficiently large to retain the characters of the spin-polarized surface states, while the bulk continua are replaced by densely populated, but experimentally resolvable, quantum well states that are spin-unpolarized in centrosymmetric cases [9]. The surface states now must disperse and connect to the quantum well states and therefore lose their spin polarization in the process by bulk symmetry requirements. The nature of this passage, relevant to spin transport and relaxation in the ballistic regime, is the focus of this paper.

We choose a simple model system, Sb films, for this investigation for two reasons. Firstly, the semimetal Sb shares the same topological order as $Bi_{1-x}Sb_x$ $(0.07 < x < 0.2)$ [5,10], the first material identified as a three-dimensional topological insulator [11]. Sb possesses a pair of Rashba-type spin split surface bands within its bulk band gap. Unlike other Rashba systems such as Au films [10], the two surface bands in Sb are connected to the conduction band and the valence band separately. The resulting gapless configuration of the surface bands gives rise to a single Dirac cone, which is the signature of nontrivial topological order. Secondly, recent studies

of Bi films [12] also show entanglement between the surface states and quantum well states and merit a comparison. However, Bi is topologically trivial; it has a more complicated band structure involving mixing of surface and bulk bands near the zone center [13,14]. The complexity impedes a straightforward demonstration of the passage from the spin polarized surface states to quantum well states. Sb films present a much simpler case.

The spin-split surface states of bulk Sb samples have been studied by angle-resolved photoemission (ARPES) before, but these states are observable only near the surface zone center [15,16,17,18]. From the fabrication standpoint, making smooth thin films that preserve the surface spin properties presents a technical challenge. Through experimentation, we have found that Sb films grown on the usual Si(111) substrates are rough. Instead, we first prepared a Bi buffer layer on the Si(111) substrate to support the growth of ultrasmooth Sb films (see supplementary document [19] for details including the use of a Bi-terminated Si(111)-$\sqrt{3} \times \sqrt{3} - R30°$ surface [20,21] for smooth Sb film growth). Bulk Sb has the rhombohedral A7 crystal structure, which is essentially a distorted fcc NaCl structure [22,23]. Films of Sb studied here are (111)-oriented and consist of a stack of bilayers (BL), each of which resembles a buckled graphene sheet. The surface Brillouin zone is a simple hexagon [19].

ARPES mapping along the $\overline{\Gamma} - \overline{M}$ direction of the band structure of a 20 BL (~79 Å) Sb film reveals a rich structure of subbands as a function of the in-plane wave vector k_x, as seen in Fig. 1(a). Figure 1(b) shows the same data differentiated twice along the energy axis. This differentiation effectively removes a background and enhances the contrast for a better visualization of the band dispersions. For comparison, Fig. 1(c) shows the results from a

first-principles calculation; the film is assumed to be freestanding for simplicity. Substrate effects including the modification of the surface states at the interface (not observable by photoemission) and a possibly tiny splitting of the quantum well subbands [24] are thus ignored here, but these do not affect our main conclusions as discussed in [19].

Two bands that have been identified as surface states near the zone center in bulk Sb are labeled A and B in Fig. 1(c). They are degenerate at the surface zone center $\bar{\Gamma}$, but separate in energy elsewhere by spin-orbit coupling because of the surface potential gradient (Rashba effect). The shading in the figure indicates the bulk band continua (thick-film limit). A gap separates the valence and conduction bands throughout the entire zone, which makes Sb a semimetal. The calculated gap is somewhat smaller than the experimental results [11]. For bulk Sb, the upper and lower surface states merge with the conduction and valence bands, respectively, and are observable only near $\bar{\Gamma}$. In the film, the bulk continuum is replaced by quantum-well states, and calculation shows these two states remaining distinct all the way to the zone boundary at $\bar{M}$. The solid curves in Fig. 1(e) indicate schematically the portions of the two states above the Fermi level based on a comparison between theory and experiment. The dashed curve Q indicates the topmost quantum well subband below states A and B. It serves as a reference for connecting the two visible pieces of state B, which lie next above Q. Likewise, the two visible pieces of state A in Fig. 1(e) are connected as they lie next above B. In bulk Sb, the states A and B are not observed near the zone boundary by photoemission, but in the film they are seen and should correspond to quantum well states, as verified by calculation (see below). The $\bar{M}$ point is a special "time-reversal invariant" point in reciprocal space. The two states remain separate in

energy at $\bar{\mathrm{M}}$, which is a necessary, but not a sufficient, condition for nontrivial topological order [4,11,19,25].

Quantum well states in freestanding Sb films are, however, spin-unpolarized, because they are derived from bulk states that are invariant under time-reversal (**T**) and space-inversion (or parity, **P**) operations. Thus, each quantum well state is doubly degenerate relative to spin. The question is: how do the two spin-split surface states get connected to spin-degenerate pairs of quantum well states across the band edges? An important clue is revealed by turning off the spin-orbit coupling in the calculation (Fig. 1(d)), thus rendering the system topologically trivial. The subband structure and the bulk gap remain largely unaffected, but the two surface states A and B become degenerate within the gap. Each state A and B is additionally doubly degenerate because of the two surfaces; the total degeneracy is thus four-fold. Outside the gap, the two connecting quantum well states remain separate. Thus, the energy separation of the two quantum well states is not a consequence of spin interaction. It must arise from differences in the spatial parts of the wave functions that lead to different charge density patterns.

An explanation is offered by the schematic diagram in Fig. 2 that shows the charge and spin characters of the surface states of a 20 BL Sb film. At the zone center, there are four degenerate surface states; each of the two surfaces (left L and right R) of the film contains two spin degenerate surface states. For each surface, the spin degeneracy is lifted away from $\bar{\Gamma}$ (Fig. 2(a)). Consider the four points on the dispersion relations, A, A', B, and B', with $k_x = \pm 0.1 |\overline{\Gamma\mathrm{M}}|$. Each surface state is characterized by a decay length (Fig. 2(b)). The two states on the right surface, A_R and B_R, are spin polarized in opposite directions, along $-y$ and $+y$, respectively. They

are related to the two states on the left surface, A_L and B_L, by $A_L = \mathbf{TP}A_R$ and $B_L = \mathbf{TP}B_R$. For the two states on the same surface but with negative k_x, the relationships are $A_R{}' = \mathbf{T}A_R$ and $B_R{}' = \mathbf{T}B_R$. The actual charge and spin distributions of the four states from the calculation are presented in Fig. 2(c).

As k_x increases, the surface states move toward the bulk band continua. Their decay lengths increase as illustrated by the calculated plane-averaged charge densities for a 20 BL Sb film (Fig. 3). Near the edges of the band gap, each pair of degenerate surface states associated with the two surfaces (e.g., A_L and A_R) begin to overlap across the central plane of the film. They remain degenerate because of their opposite spin orientations. However, the spatial overlap leads to a cancellation of the spin polarizations. Eventually, they combine into a quantum well state pair, doubly degenerate with respect to spin, and with a charge density distribution resembling a standing wave bounded within the film. This manner of passage from surface states to quantum well states allows the spin polarization to switch smoothly across the band edges. The degeneracy of the two surface states associated with spatial separation (left and right surfaces) evolves into spin degeneracy for the two quantum well states with identical spatial wave functions.

With the spin-orbit coupling turned off in the calculation, the four states A_R, A_L, B_R, and B_L are degenerate within the gap (Fig. 1(d)). They split into two spin-degenerate pairs of quantum well states across the band edges, one pair derived from a mixture of A_R and A_L, and the other from a mixture of B_R and B_L. The splitting can be understood in terms of how the two surface states from the two surfaces interact in real space when their decay lengths are long enough for

them to overlap. The interaction leads to a mixing that can be either in phase or out of phase, resulting in an antinode or node at the midpoint of the film. The energy splitting is the usual even-odd splitting familiar from surface state calculations for films that are sufficiently thin for the states associated with the two surfaces to couple, and this mechanism applies only to states having the same spin. The calculated charge density functions in Fig. 3 reveal the differences in the nodal structures of the quantum well states [19].

The passage from surface states to quantum well states, with very different charge distributions, can be characterized by the charge separation function defined below for each of the two states A and B:

$$\Delta C\left(k_{x}\right)=\frac{2}{D}\sum_{i=L,R}\left\langle\Psi_{i}\left(k_{x}\right)\middle|\left(\rho\,|\,z\,|\right)\middle|\Psi_{i}\left(k_{x}\right)\right\rangle-1, \tag{1}$$

where D is the film thickness, ρ is the normalized charge density operator, $z = 0$ is at the midpoint of the film, and the summation is for the two degenerate states associated with the two surfaces. It ranges from 0 (uniform charge distribution) to 1 (charge concentrated at the surfaces at $z = \pm D/2$). The results from the calculation, presented in Fig. 4, show a smooth transition across the band edges. Likewise, a spin separation function can be defined:

$$\Delta S\left(k_{x}\right)=\frac{2}{\hbar D}\sum_{i=L,R}\left\langle\Psi_{i}\left(k_{x}\right)\middle|s_{y}z\middle|\Psi_{i}\left(k_{x}\right)\right\rangle, \tag{2}$$

where s_y is the spin operator along y, the only direction yielding a nonzero value based on the Rashba effect [26]. This quantity is normalized to ± 1 for a fully spin-polarized **TP** pair concentrated at the two film surfaces, and its sign indicates the spin orientation of the state on the right (positive z) surface. The calculated results in Fig. 4 show a transition from oppositely

polarized surface states at the two surfaces to unpolarized quantum well states, with a trend of transition very similar to that of the charge separation.

Topological materials are of interest in that the surface states pinned at opposite surfaces possess opposite transverse spin orientations. Such spatial separation of spin and associated charge, without an applied magnetic field, is an essential ingredient for realizing the quantum spin-Hall effect [27,28]. Thin films of these materials offer flexibility for device design and integration. This work employs a special Bi interface layer to prepare topologically nontrivial Sb films of excellent structural quality on standard Si substrates. A comparison between theory and experiment allows us to explore the interplay between quantum confinement and spin separation, which offers a path forward for utilizing topological materials for thin film applications.

REFERENCES

[1] M. Z. Hasan and C. L. Kane, Rev. Mod. Phys. **82**, 3045 (2010).

[2] X.-L. Qi and S.-C. Zhang, arXiv:1008.2026v1 (2010).

[3] B. A. Bernevig, T. L. Hughes, and S.-C. Zhang, Science **314,** 1757 (2006).

[4] L. Fu, C. L. Kane, and E. J. Mele, Phys. Rev. Lett. **98**, 106803 (2007).

[5] L. Fu and C. L. Kane, Phys. Rev. B **76**, 045302 (2007).

[6] D. Hsieh, D. Qian, L. Wray, Y. Xia, Y. S. Hor, R. J. Cava, and M. Z. Hasan, Nature **452**, 970 (2008).

[7] Y. Xia, D. Qian, D. Hsieh, L. Wray, A. Pal, H. Lin, A. Bansil, D. Grauer, Y. S. Hor, R. J. Cava, and M. Z. Hasan, Nature phys. **5**, 398 (2009).

[8] Y. L. Chen, J. G. Analytis, J.-H. Chu, Z. K. Liu, S.-K. Mo, X. L. Qi, H. J. Zhang, D. H. Lu, X. Dai, Z. Fang, S. C. Zhang, I. R. Fisher, Z. Hussain, and Z.-X. Shen, Science **325**, 178 (2009).

[9] T.-C. Chiang, Surf. Sci. Rep. **39**, 181 (2000).

[10] D. Hsieh, Y. Xia, L. Wray, D. Qian, A. Pal, J. H. Dil, J. Osterwalder, F. Meier, G. Bihlmayer, C. L. Kane, Y. S. Hor, R. J. Cava, and M. Z. Hasan, Science **323**, 919 (2009).

[11] D. Hsieh, L. A. Wray, D. Qian, Y. Xia, Y. S. Hor, R. J. Cava, and M. Z. Hasan, arXiv:1001.1574v1 (2010).

[12] T. Hirahara, T. Nagao, I. Matsuda, G. Bihlmayer, E. V. Chulkov, Yu. M. Koroteev, P. M. Echenique, M. Saito, and S. Hasegawa, Phys. Rev. Lett. **97**, 146803 (2006).

[13] G. Bian, T. Miller, and T.-C. Chiang, Phys. Rev. B **80**, 245407 (2009).

[14] Yu. M. Koroteev, G. Bihlmayer, E. V. Chulkov, and S. Blügel, Phys. Rev. B **77**, 045428 (2008).

[15] L. M. Falicov and P. J. Lin, Phys. Rev. **141** 562 (1966).

[16] T. Kadono, K. Miyamoto, R. Nishimura, K. Kanomaru, S. Qiao, K. Shimada, H. Namatame, A. Kimura, and M. Taniguchi, Appl. Phys. Lett. **93**, 252107 (2008).

[17] K. Sugawara, T. Sato, S. Souma, T. Takahashi, M. Arai, and T. Sasaki, Phys. Rev. Lett. **96**, 046411 (2006).

[18] H. Höchst and C. R. Ast, J. Electron Spectrosc. Rel. Phenom. **137–140,** 441 (2004).

[19] Online supplementary document.

[20] J. M. Roesler, T. Miller, and T.-C. Chiang, Surf. Sci. Lett. **417**, L1143 (1998).

[21] I. Gierz, T. Suzuki, E. Frantzeskakis, S. Pons, S. Ostanin, A. Ernst, J. Henk, M. Grioni, K. Kern, and C. R. Ast, Phys. Rev. Lett. **103**, 046803 (2009).

[22] Y. Liu and R. E. Allen, Phys. Rev. B **52**, 1566 (1995).

[23] H.-J. Zhang, C.-X. Liu, X.-L. Qi, X.-Y. Deng, X. Dai, S.-C. Zhang, and Z. Fang, Phys. Rev. B **80**, 085307 (2009).

[24] J. Hugo Dil, F. Meier, J. Lobo-Checa, L. Patthey, G. Bihlmayer, and J. Osterwalder, Phys. Rev. Lett. **101**, 266802 (2008).

[25] K. K. Gomes, W. Ko, W. Mar, Y. Chen, Z.-X. Shen, and H. C. Manoharan, arXiv:0909.0921v2 (2009).

[26] Y. A. Bychkov and E. I. Rashba, J. Phys. C **17,** 6039 (1984).

[27] C. L. Kane and E. J. Mele, Phys. Rev. Lett. **95**, 226801 (2005).

[28] X.-L. Qi and S.-C. Zhang, Physics Today **63**, 33 (2010).

FIG. 1. (a) ARPES data taken at 22 eV from a 20 BL Sb film grown on a Bi buffer layer. (b) Second derivatives of the data along the energy axis. (c,d) Calculated band structure for a freestanding 20 BL Sb film with and without spin-orbit coupling, respectively. (e) Data near the Fermi level, where the solid curves indicate schematically the surface bands A and B above the Fermi level by comparison with theory. The curve Q indicates the topmost quantum well subband below the states A and B.
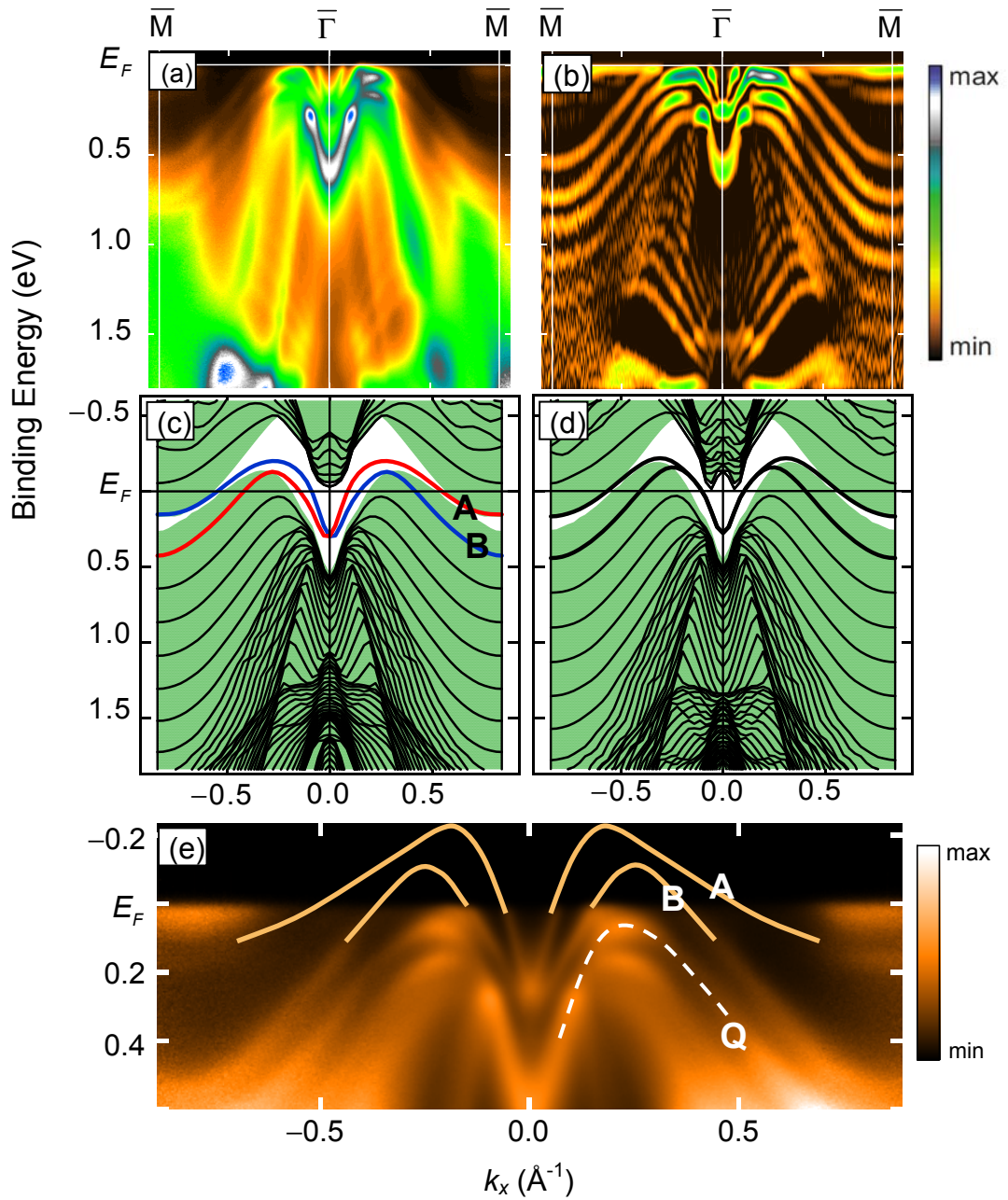
FIG. 2 (Color online). Charge and spin distributions of surface states of a 20 BL Sb film. (a) Surface band structures near the zone center with four points A, A', B, and B' marked at $k_x = \pm 0.1|\overline{\Gamma M}|$. Each point corresponds to two degenerate surface states located at the opposite surfaces of the film. (b) Schematic charge densities and spin orientations for states A, A', B, and B' on the two surfaces. The spin orientations are indicated. (c) Calculated charge density $\langle \rho \rangle$ and spin density $\langle s_y \rangle$ along z for the four surface states at $k_x = +0.1|\overline{\Gamma M}|$.
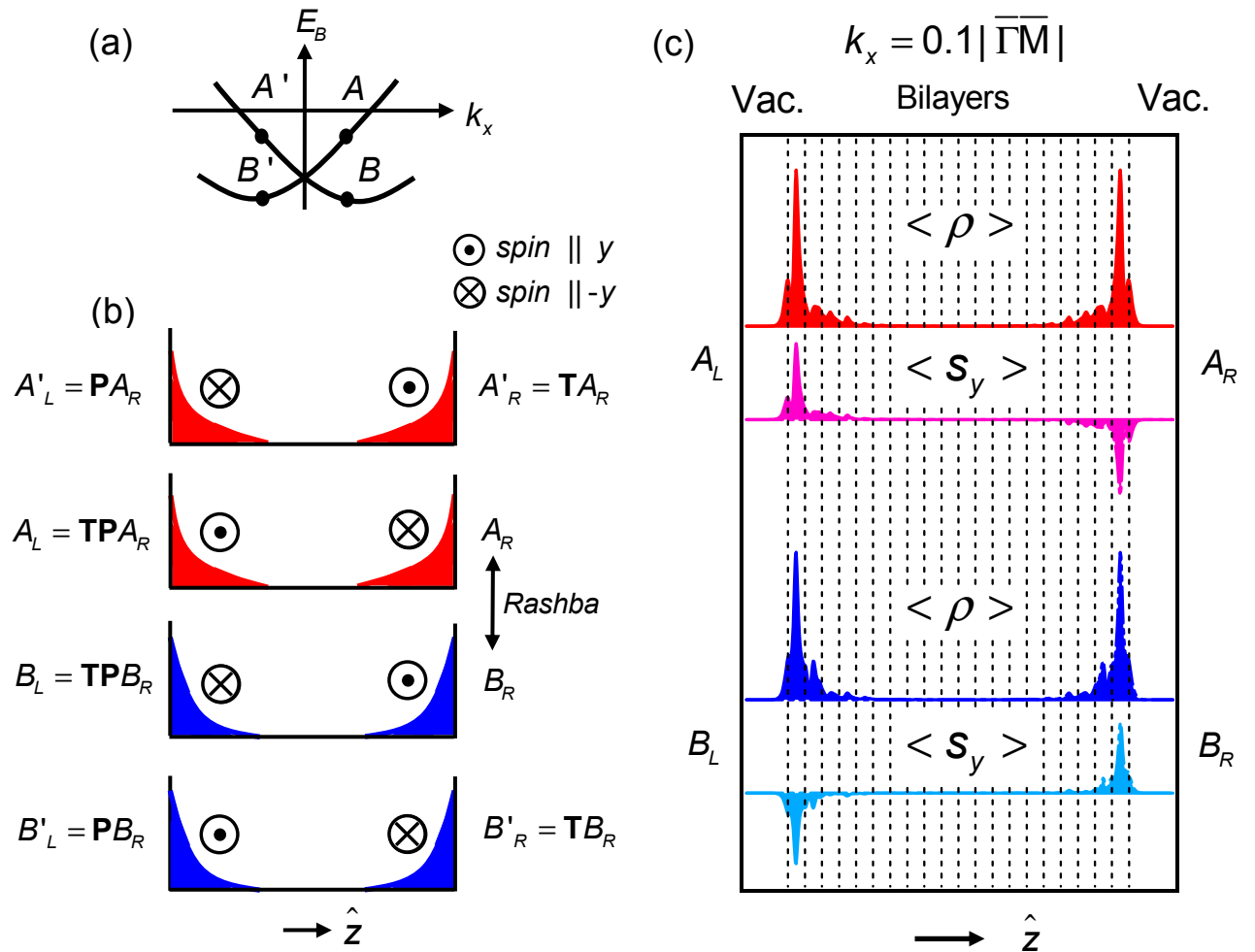
FIG. 3 (Color online). Calculated plane-averaged electronic charge densities in a 20 BL Sb film for (a) state A_R and (b) state B_R. The central plane of the slab is marked by a triangle. (c,d) Corresponding results computed without spin-orbit coupling.
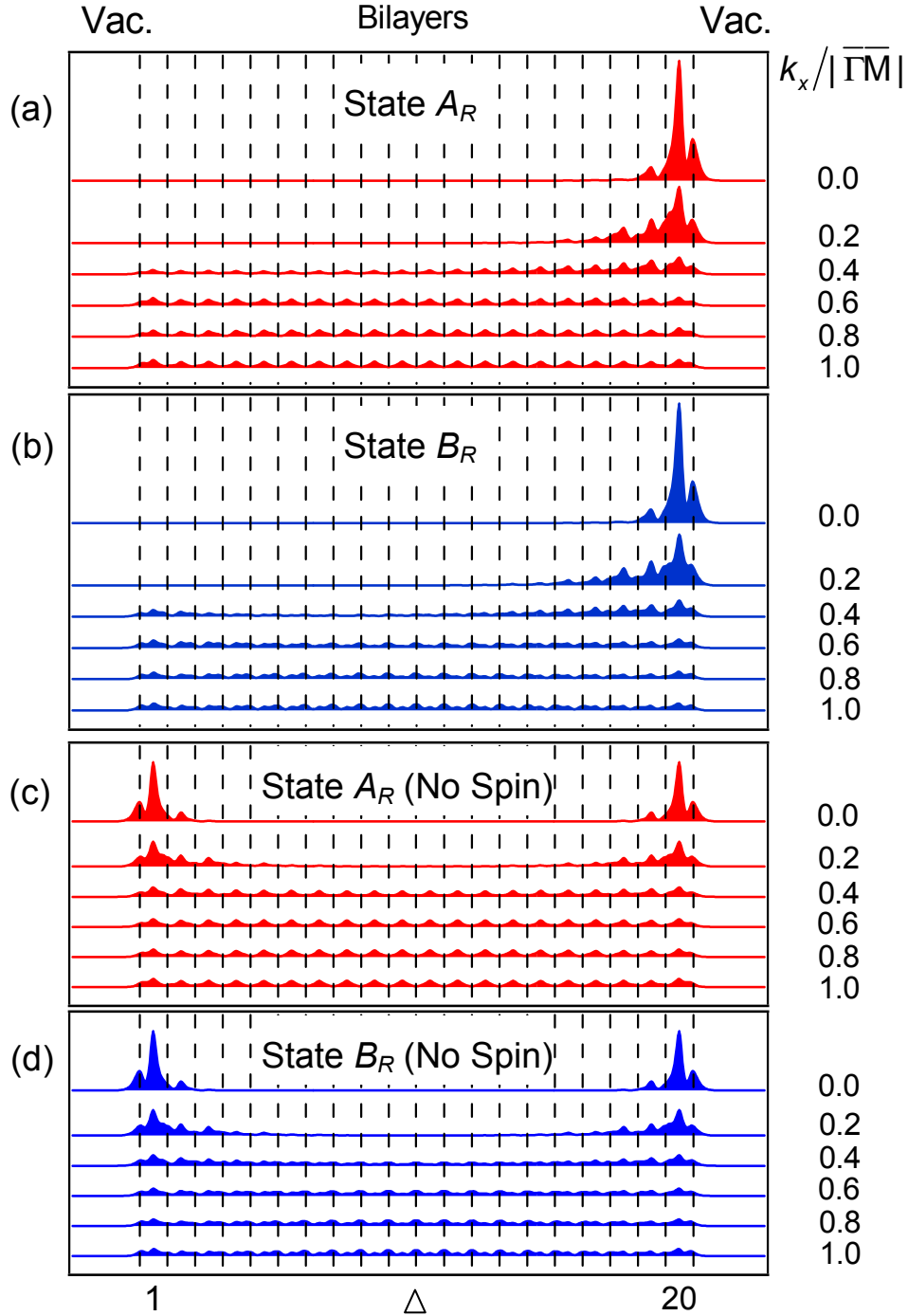
FIG. 4 (Color online). (a) Calculated charge separation function, or the normalized absolute charge moment, as a function of k_x for a 20 BL Sb film. (b) The corresponding spin separation function, or the normalized spin moment, along y.